



Photoluminescence in silicon/silicon oxide films produced by the Pulsed Electron Beam Ablation technique

M. Araya^a, D.E. Díaz-Droguett^b, M. Ribeiro^c, K. F. Albertin^e, J. Avila^d, V.M. Fuenzalida^d, R. Espinoza^a, D. Criado^{a,f,*}

^a Departamento de Ciencias de los Materiales, FCFM, Universidad de Chile, Av. Tupper 2069, Santiago, Chile

^b Pontificia Universidad Católica de Chile, Santiago, Chile

^c EPUSP, Universidade de São Paulo, CP 615478, CEP 5424–970, São Paulo, SP, Brazil

^d Departamento de Física, FCFM, Universidad de Chile, Casilla 487–3, Santiago 6511226, Chile

^e CECS, Universidade Federal do ABC – UFABC, CEP 09.210-170, Santo André, SP, Brazil

^f CCNH, Universidade Federal do ABC – UFABC, CEP 09.210-170, Santo André, SP, Brazil

ARTICLE INFO

Article history:

Received 25 July 2011

Received in revised form 13 December 2011

Available online 17 January 2012

Keywords:

Electron beam;

Silicon oxide;

Photoluminescence

ABSTRACT

In this work we report studies of the photoluminescence emission in samples based on Si/SiO_x films deposited by the Pulsed Electron Beam Ablation (PEBA) technique. The samples were prepared at room temperature using targets with different Si/SiO₂ concentrations. The samples were characterized using X-ray Absorption Edge Spectroscopy (XANES) at the Si–K edge, Raman spectroscopy, Photoluminescence (PL) and X-ray Photoelectron Spectroscopy (XPS). The concentration of a-Si and nc-Si in the film was dependent on the silicon concentration in the target. It was also observed that the PL is strongly dependent on the structural amorphous/crystalline arrangement.

© 2011 Published by Elsevier B.V. All rights reserved.

1. Introduction

The photoluminescence in silicon nanoparticles has been widely studied since the discovery of bright emission in porous silicon at room temperature in the 1990s [1]. One area of application of these nanoparticles is in optoelectronic devices due to the possibility of producing optical and electronic devices using the current silicon-based technology, hence greatly reducing manufacturing costs and the problems arising in the integration of optical and microelectronic devices [2]. The challenge to use silicon as an emitter device is to produce tunable PL in the entire visible range [3]. Several techniques have been employed to obtain silicon nanoparticles, such as sputtering [4–6], evaporation [7,8], PECVD [2,9], ionic implantation [10], among others. In general, these techniques produce a silicon-rich material by deposition or growth followed by annealing at high temperature to form silicon nanoparticles [2]. However, the high temperature works against the integration with electronic devices due to the diffusion of dopants [11].

In this work, Si nanoparticles were produced by the PEBA technique. This technique presents some advantages compared to UV-laser ablation such as low deposition cost, good thickness control, possibility of producing films of complex stoichiometry (such as high-

Tc superconductors, intermetallic alloys and glasses), the absence of the dangerous gasses pervading CVD techniques [12], and low deposition temperature. This technique is a process in which a high power electron beam (15–20 KV) is pulsed producing the volatilization of the impacted region of the material. In this work we study the formation of silicon clusters in the film and the influence of the deposition process on the photoluminescence.

2. Experimental

We prepared targets for the PEBA technique starting from powder mixtures of silicon dioxide 99.5% metal basis and silicon 99.5%, crystalline, both –325 mesh in size (Alfa Aesar). Three Si:SiO₂ powder ratios were used, as shown in the Table 1. After mixing, the powders were compacted by a press and sintered in argon ambient at 1100 °C.

Before the deposition, the deposition chamber was pumped to 0.01 Pa, while the PEBA process was performed under Argon, at 1.33 Pa approximately. The current was fixed at 1 mA and the voltage at 18–20 KV. The samples were deposited at room temperature onto a copper wafer.

The samples were characterized using X-ray photoelectron spectroscopy (XPS), in a Physical Electronics 1257 system. A Gaussian peak shape was assumed for each element fitted. The XANES at the Si–K edge measurements were conducted at the SXS beam line of the Brazilian Synchrotron Light Laboratory (LNLS, Campinas, Brazil) in the 1835–1855 eV range. A micro Raman spectrometer was used to determine the changes in the Si–Si bonding within the material.

* Corresponding author at: Centro de Ciências Naturais e Humanas, Universidade Federal do ABC, CEP: 09.210.170, Santo André, SP, Brazil. Tel.: +55 11 49968362; fax: +55 11 49960090.

E-mail address: denise.criado@ufabc.edu.br (D. Criado).

Table 1
Powder ratio used in the target production.

Name	Si:SiO ₂ ratio	
	Si	SiO ₂
S12	1	2
S11	1	1
S21	2	1

The equipment utilized was a Renishaw spectrometer with 1 μm spatial resolution, equipped with a CCD detector and optical microscope, at Instituto de Química, USP, Brazil. The same equipment was used for the photoluminescence measurements, performed with a 514.5 nm argon laser. All the measurements were performed at room temperature.

3. Results

XPS analyses were performed in the targets after sintering and in the deposited films. The Si 2p level spectra for the three as-prepared targets are presented in Fig. 1. The target with the higher SiO₂ concentration, S12, (Fig. 1a) presents a clear separation between Si⁴⁺ (associated to SiO₂) and Si⁰ (associated to metallic Si). A small amount of the Si²⁺ oxidation state can also be observed, indicating a weak reaction of the powders during sintering.

The S11 target with the equal concentrations of Si and SiO₂, (Fig. 1b) shows a higher degree of reaction than the S12 target, presenting all the intermediate oxidation states between Si⁰ and Si⁴⁺.

For the target with the higher Si concentration in the powder mixture, S21, (Fig. 1c), the Si²⁺ oxidation state was not observed, but it showed all the other ones (Si⁰, Si¹⁺, Si³⁺ and Si⁴⁺), with intensity ratios of the signals associated to Si⁰, Si¹⁺ and Si³⁺ with respect to Si⁴⁺ higher than the previous targets. This fact could be related to a higher silicon proportion contained in the target which would favor the reaction between the Si and SiO₂ powder due to the high affinity of silicon with oxygen.

The binding energies of the oxidation states found in the S12 and S11 targets are higher than the values reported in the literature [13], in special the ones associated to Si²⁺, Si³⁺ and Si⁴⁺. We believe that these higher values are due to a charging effect of the samples (targets) when they were analyzed by XPS. Nonetheless, values closer to the reported data were found in the S21 target.

The XPS results for the as-deposited samples (using the targets above) are shown in Fig. 2. We can see from Fig. 2a that the spectra of the deposited samples are different from those of the targets, presenting a unique broad band with a left shoulder. Fitting of the

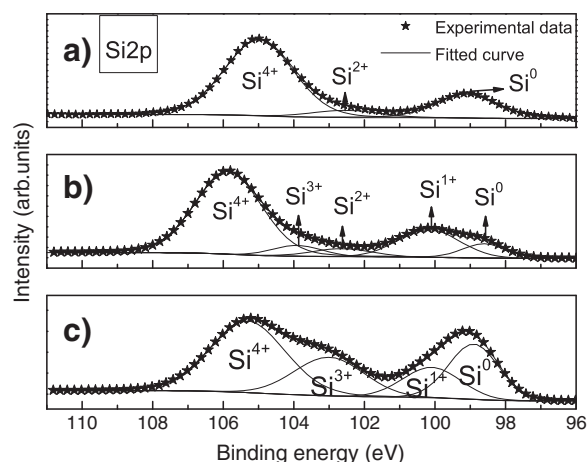


Fig. 1. Si 2p spectra from the targets after sintering: a) S12, b) S11, c) S21.

spectra demonstrate the presence of three peaks, related to the Si³⁺ and Si²⁺ oxidation states and to Si⁰. The presence of SiO₂ bonding was not detected. Here, the binding energies for Si³⁺ and Si²⁺ are closer to the reported values [13] probably due to a lower charging effect in these samples which were deposited onto copper substrates. A typical fit for these samples is depicted in Fig. 2b corresponding to the S21 sample.

The XPS results are very similar for the two samples with lower Si content in the powder mixture, samples S12 and S11. For the sample with higher Si content, S21, it is possible to observe a higher Si⁰ contribution compared to the spectra of the other samples (Fig. 2a).

The spectrum corresponding to the O1s level was very similar for all samples (Fig. 2c), presenting the contribution of the peak related to Si—(SiO₃) bonding. It shows that oxygen completes its bonds only with silicon in the Si—O—Si bridge, as in SiO₂ (Fig. 2d). There is a small contribution of Si—(Si₂O₂) and a small presence of O—H groups.

The XANES results at the Si—K edge for the three deposited films are shown in Fig. 3. All spectra were normalized for a better comparison. The spectra corresponding to crystalline-Si and thermal SiO₂ standard samples are also shown for comparison, in which the absorption edges are present at 1839 and 1846 eV, respectively. The 1st derivative of the spectra was computed for better comparison between the absorption edges (Fig. 3b). We can observe two well-defined absorption edges at the same energies: 1839 and 1845 eV in all deposited samples. The 1839 eV peak is related to Si—Si bonds, while the 1845 eV peak can be related to the reduced SiO³⁺, as shown in the XPS results. Among those absorption edges there is a less-defined absorption edge, which can be related to the SiO²⁺ oxidation state. The sample with the higher Si content presents the higher intensity at the Si—Si energy.

The Raman spectra for the as-deposited samples are shown in Fig. 4. To assist in the Raman analysis of the samples, measurements on crystalline silicon and on an amorphous silicon film were also carried out for comparison.

A band at 480 cm⁻¹ and at 520 cm⁻¹ corresponding to Si—Si bonds vibrations as a-Si clusters and as c-Si arrangement respectively is observed in Fig. 4. For bulk amorphous silicon the signal due to Si—Si bonds is a wide band centered at 480 cm⁻¹ and for small amorphous silicon clusters this signal shifts towards a lower wavenumber. For bulk crystalline silicon, Si—Si bonds arranged as silicon single crystal peak appears at 520 cm⁻¹, and nano- or micro-crystals appear in the range from 490 cm⁻¹ to 516 cm⁻¹ as observed in the S11 and S21 samples. The sample S12 presents a narrow band at 514 cm⁻¹, which can be attributed to the presence of small silicon nanocrystals.

The photoluminescence spectra of all samples are shown in Fig. 5 and the PL spectrum of the copper substrate is also added, as observed it does not interfere with the results.

The S12 sample shows a band at 1.4 eV and at 2.1 eV. The small linewidth PL band at 1.4 eV should be attributed to the presence of nc-Si also observed as a narrow band at 514 cm⁻¹ in the Raman result.

For samples S12 and S11 the intensity of the band at 1.4 eV is higher than the other band, which does not occur for S21 sample. A wide PL band centered at 1.9 eV for the S21 sample is observed.

4. Discussion

The phase separation and the small size of the silicon clusters are responsible for the optical modifications of the photoluminescence of silicon based films, and Raman spectroscopy has shown to be very sensitive to the local atomic arrangement in the study of those films [14,15].

The shape of the spectrum permits to evaluate the presence of silicon excess dispersion in the samples. It is observed that the

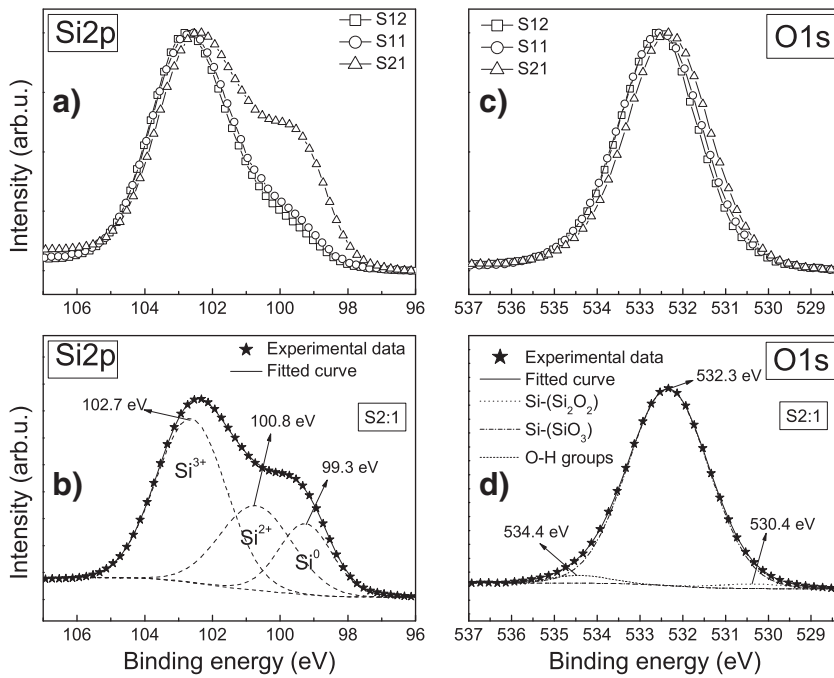


Fig. 2. XPS spectra of the as-deposited samples: a) Si 2p level and b) O1s level; c) and d) correspond to the Si2p and O1s levels in the S21 deposited sample, respectively.

amount of redshift and linewidth broadening of the Raman line depends on the silicon clusters size dispersion. In bulk silicon a maximum small linewidth shape peak at 520 cm^{-1} is observed, corresponding to the optical-phonon frequency. On the other hand, for nanostructured silicon, all the phonons of the dispersion relation will contribute to the Raman signal from all the nanocrystals and clusters, causing broadening in the Raman signal to lower frequencies when they become smaller.

It is observed that the spectra for the S11 and S21 samples present a pronounced Raman signal from 470 cm^{-1} to 480 cm^{-1} indicating the presence of small a-Si clusters and the peak at 516 cm^{-1} indicates the presence of silicon aggregation as nanocrystals. The presence of the band centered at 480 cm^{-1} is observed for both samples but being more symmetric for the higher silicon content sample indicating a higher volume fraction of a-Si clusters, situation also confirmed by the XANES and XPS results. As the silicon content in the films decreases, the Raman spectra become more asymmetric

shifting to lower frequencies to indicate dispersion of small a-Si clusters in small volume fraction. For the S12 sample there is a small evidence of Si—Si bonds at 480 cm^{-1} and it also presents a peak at 514 cm^{-1} indicating the presence of Si-nc which is also observed in the XANES result by the presence of a shoulder in the c-Si region. In summary, all the samples presented a-Si clusters in the as deposited condition; the Raman results could be associated to the XANES results that indicated a more pronounced phase separation with the enhancement of the silicon content in the samples.

The as-prepared films present amorphous silicon and crystalline silicon. The presence of a-Si is observed in the Raman spectra by the separation between the c-Si and a-Si signals, and also in the XANES spectra by the identification of Si and SiO_x suboxides. In order to correlate these results with the PL, the c-Si/a-Si ratio was extracted by deconvoluting the crystalline and amorphous contributions to the Raman signal, as shown in the insert of Fig. 4 (an example of the deconvolution in sample S21). The c-Si/a-Si ratio for sample S12 was higher than 90%, indicating a small amorphous contribution to the Raman signal, and, consequently, a large contribution of nc-Si

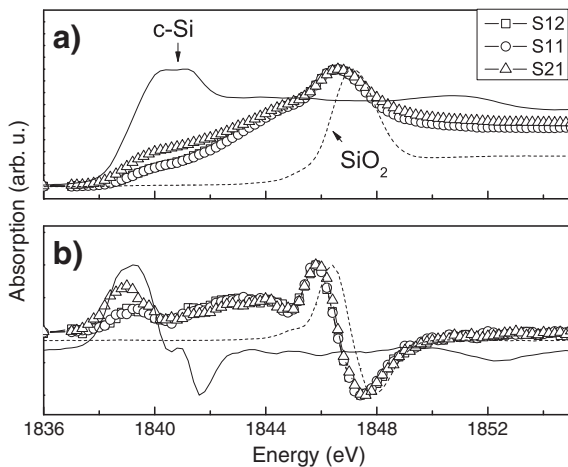


Fig. 3. a) XANES at Si-K edge for samples deposited with the initial mixture ratio of Si:SiO₂ according to Table 1 and b) the 1st derivate of the spectra for better comparison between the absorption edges.

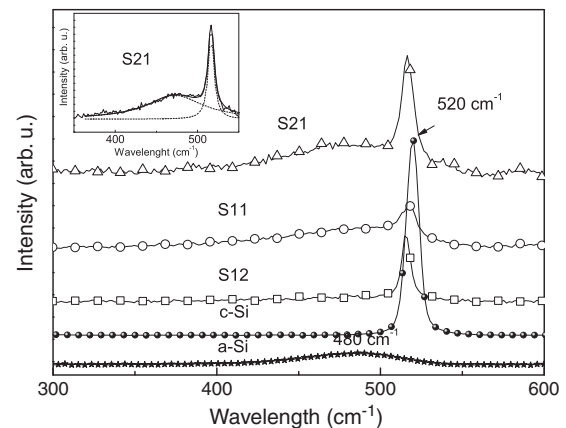


Fig. 4. Raman spectra for all as-deposited samples. The inserted figure shows the deconvolution of a-Si and c-Si contributions in sample S21.

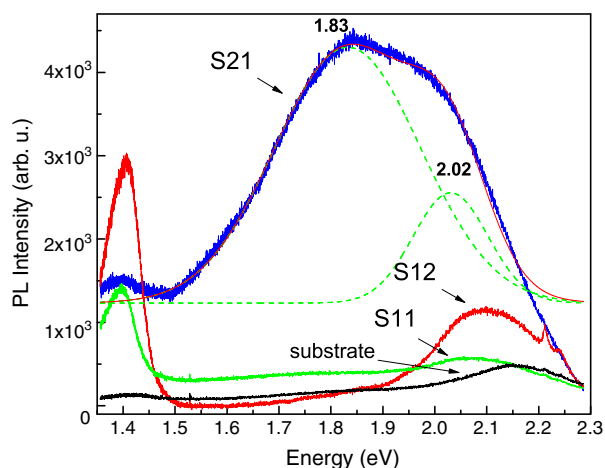


Fig. 5. Photoluminescence spectra for all samples deposited at 514.5 nm.

to the PL spectrum. For the sample with the intermediate chemical composition, S11, the ratio c-Si/a-Si was around 22%, which shows that there is more amorphous phase and fewer Si crystals than in S12 sample. The sample S21 presents a c-Si/a-Si ratio of 35%, which indicates an intermediate amorphous content. The PL response could be explained as the contribution of a-Si clusters and nc-Si of different sizes, since the deposition process used in this work inherently leads to different clusters sizes (a-Si and c-Si), and all these different cluster sizes can contribute to produce a wide PL signal.

All samples present an infrared PL peak at 1.40 eV. The IR PL band has been discussed in several works [16–19] and it has been rationalized on the basis of the quantum confinement model for nc-Si with sizes less than 5.0 nm. This statement agrees with c-Si/a-Si ratio in all samples, which for sample S12 is the highest. For this sample the PL spectrum presents the highest intensity, which could be related to a higher concentration of small Si nanocrystals. The samples S21 and S11 both exhibit an IR PL intensity lower than sample S12, in agreement with their c-Si/a-Si ratios, 35 and 22%, respectively.

The samples S12 and S11 both present similar silicon and SiO_x contents as shown in the XANES and XPS analyses. On the other hand, the PL spectra of the same two samples (S12 and S11) present two bands, at 1.40 eV and approximately 2.10 eV, respectively. The latter band has a small contribution centered at 2.15 eV coming from the copper substrate. The intensity ratio $I_{1.40\text{eV}}/I_{2.10\text{eV}}$ for both samples was essentially the same, which could be related to a similar silicon neighborhood. The 2.10 eV peak has been previously attributed to defects in the SiO₂ [20]. The difference among these samples is mainly in the c-Si/a-Si ratio, which is evidenced in both the Raman results and the PL results as the intensity at 1.4 eV (nc-Si) and the wide band between 1.5–1.9 eV (a-Si). We can see that the sample S12 presents a high 1.4 eV intensity and a very small intensity at 1.5–1.9 eV band, showing a high nc-Si contribution. On the other hand, the S11 sample presents a lower intensity at 1.4 eV and a higher intensity at 1.5–1.9 eV than the S12 sample, showing a higher a-Si contribution.

To understand the S21 wide band we can correlate our results with porous silicon experiments found in the literature [21,22]. For large silicon crystallites ($>> 10$ nm) the PL cannot be related to quantum confinement effects. However, we attribute the PL in the visible range to a-Si clusters of different sizes as well as the presence of interfacial defects. The PL spectrum of sample S21 was deconvoluted into two Gaussian curves centered at 1.83 eV and 2.03 eV, which in the literature have been attributed to confined nanostructured silicon and SiO related defects, respectively [23]. Moreover, the 1.83 eV peak has been attributed to emission in small a-Si clusters, while the 2.03 eV peak has been attributed to radiative recombinations at

the dioxide defects. M. Molinari [24] discussed the influence of a transition between a-Si and nc-Si (induced by an annealing process) on the PL emission. It was shown that the luminescence intensity and the confinement energy were higher in the crystalline state than in the amorphous state. M. Estes [25] used an energy diagram to explain the room temperature luminescence observed in a-Si spheres of different sizes. In bulk materials, carriers thermalize to the lowest energy states, but spatially confining carriers to even smaller volumes, as in small a-Si clusters, have the effect of increasing the average energy of the lowest energy state as well as reducing the probability of encountering nonradiative recombination centers. The gap of a-Si can be explained by disorder-induced localized states extending into the high gap matrix. These localized states feel the confinement effect because they are weakly localized [24]. Although the sample S11 presents the lowest c-Si/a-Si ratio, it does not contain the largest amount of a-Si, thus explaining why this sample does not show the highest PL intensity at approximately 1.8 eV. This sample also has a higher SiO³⁺ and SiO²⁺ content than the sample S21, as can be seen in the XPS results. On the other hand, the sample S21 has a higher Si⁰ content, so Si-cluster of different sizes are formed (in a broad size distribution), whether c-Si or a-Si, according to the Raman analysis. This result agrees with the XANES results, which show a strong phase separation between Si–Si and Si–O for sample S21, along a higher concentration of Si–Si bonds. Moreover, the XPS results indicate that the sample S21 has a higher Si²⁺ contribution compared to the other samples, which can be related to a higher concentration of defects at the Si/SiO_x interface. In order to correlate these results, time-resolved PL measurements should be performed to separate the quantum-confinement and interfacial-recombination emission mechanisms.

5. Conclusion

We have shown the possibility of controlling the PL emission by changing the chemical composition of the targets. It was possible to obtain different structural arrangement in the film, as nc-Si, amorphous silicon, and consequently, different PL emission, using the PEBA technique at room temperature. From the structural point of view, all samples can be thought as a composite material in which the size and density of the silicon clusters as well the Si-nc embedded in the SiO_x matrix are modified by the silicon content.

The photoluminescence at visible range was obtained using a single-step deposition process, with no further heat treatment needed, reducing the production cost. The process at room temperature may allow the use of various types of substrates, such as plastics, polymers, etc.

Acknowledgments

The authors are grateful to the Laboratório de Espectroscopia Molecular at IQUSP for Raman spectra and to the Brazilian Synchrotron Light Laboratory—LNLS at the SXS line for XANES spectra. The authors are also grateful to the Chilean agency CONICYT for the financial support (Grant no. 11085026).

References

- [1] L.T. Canham, Appl. Phys. Lett. 57 (1990) 1046–1048.
- [2] T. Creazzo, B. Redding, E. Marchena, J. Murakowski, D.W. Prather, J. Lumin. 130 (2010) 631–636.
- [3] Q. Ma, R. Xiong, Y. Ming Huang, J. Lumin. 131 (2011) 2053–2057.
- [4] Y. So, S. Huang, G. Conibeer, M.A. Green, Thin Solid Films 519 (2011) 5408–5412.
- [5] Z. Xia, S. Huang, Solid State Commun. 150 (2010) 914–918.
- [6] A. Keffous, A. Cheriet, Y. Belkacem, N. Gabouze, A. Boukezzata, Y. Boukennou, A. Brighet, R. Cherfi, M. Kechouane, L. Guerbou, I. Menous, H. Menari, Appl. Surf. Sci. 256 (2010) 4591–4595.
- [7] B. Choi, J. Lee, K. Yatsui, S. Yang, Surf. Coat. Technol. 201 (2007) 5003–5006.
- [8] I. Bineva, D. Nesheva, Z. Aneva, Z. Levi, J. Lumin. 126 (2007) 497–502.
- [9] A. Bacoglu, A.O. Kodolbas, Ö. Öktü, J. Lumin. 130 (2010) 1730–1737.

- [10] A. Morales-Sánchez, K.M. Leyva, M. Aceves, J. Barreto, C. Domínguez, J.A. Luna-López, J. Carrillo, J. Pedraza, *Mater. Sci. Eng. B* 174 (2010) 119–122.
- [11] L.B. Ma, A.L. Ji, C. Liu, Y.Q. Wang, Z.X. Cao, *J. Vac. Sci. Technol. B* 22 (6) (2004) 2654–2657.
- [12] G. Müller, M. Konijnenberg, G. Krafft, C. Schultheiss, Forschungszentrum Karlsruhe (1994).
- [13] F. Teixeira, R. Berjoan, G. Peraudeau, D. Perarnau, *Sol. Energy* 78 (2005) 763–771.
- [14] M. Ribeiro, I. Pereyra, M.I. Alayo, *Thin Solid Films* 426 (2003) 200–204.
- [15] M. Ribeiro, I. Pereyra, *Phys. Status Solidi C* 7 (2010) 624–627.
- [16] E. Cho, M.A. Green, J. Xia, R. Corkish, P. Reece, M. Gal, *Appl. Phys. Lett.* 84 (2004) 2286–2288.
- [17] N. Korsunskaya, L. Khomenkova, V. Yukhimchuk, B. Jumayev, T. Torchynska, A. Many, E. Savir, Y. Goldstein, J. Jedrzejewski, *J. Phys. Condens. Matter* 14 (2002) 13217–13221.
- [18] T.V. Torchynska, A. Vivas Hernandez, Y. Goldstein, J. Jedrzejewski, S. Jiménez Sandoval, *J. Non-Cryst. Solids* 352 (2006) 1152–1155.
- [19] I. Stenger, L. Siozade, B. Gallas, S. Fisson, G. Vuye, J. Rivory, *Surf. Sci.* 601 (2007) 2912–2916.
- [20] T.V. Torchynska, *J. Non-Cryst. Solids* 352 (2006) 2484–2487.
- [21] T.V. Torchynska, A. Diaz Cano, M. Morales Rodriguez, L.Yu. Khomenkova, *Physica B* 350–342 (2003) 1113–1118.
- [22] T.V. Torchynska, *J. Appl. Phys.* 92 (2002) 4019–4023.
- [23] Atif Mossad Ali, Takao Inokuma, Seiichi Hasegawa, *Appl. Surf. Sci.* 253 (2006) 1198–1204.
- [24] M. Molinari, H. Rinnert, M. Vergnat, *Europhys. Lett.* 66 (5) (2004) 674–679.
- [25] M.J. Estes, G. Moddel, *Appl. Phys. Lett.* 68 (13) (1996) 1814–1816.